Combined ARPES and STM study of Pb/Au(111) Moire structure: One overlayer, two symmetries

Crepaldi, A ; Pons, S ; Frantzeskakis, E ; Calleja, F ; Etzkorn, M ; Seitsonen, A P ; Kern, K ; Brune, H ; Grioni, M

Abstract: The structural and electronic properties of a Pb monolayer (ML) grown on Au(111) are investigated by scanning tunneling microscopy (STM) and angle resolved photoelectron spectroscopy (ARPES). We find an incommensurate Moire structure with an approximate (5.77 x 5.77) R21.5 degrees. unit cell, and two rotational domains. We observe three Pb-derived bands of p orbital character. The symmetry properties and sharpness of their Fermi surfaces are remarkably different. They reflect the different degrees of hybridization of these bands with the Au(111) bulk continuum. DOI: 10.1103/PhysRevB.87.115138

DOI: https://doi.org/10.1103/PhysRevB.87.115138

Combined ARPES and STM study of Pb/Au(111) moiré: one overlayer, two symmetries

Alberto Crepaldi,[1,*] Stéphane Pons,[1,2] Emmanouil Frantzeskakis,[3] Fabian Calleja,[1] Markus Etzkorn,[1] Klaus Kern,[1,4] Harald Brune,[1] and Marco Grioni[1]

[1]*Institut de Physique de la Matière Condensée (ICPM), Ecole Polytechnique Fédérale de Lausanne (EPFL), Station 3, CH-1005 Lausanne, Switzerland*
[2]*Institut des NanoSciences de Paris (INSP), Université Pierre et Marie Curie (UPMC) - Paris 6, CNRS UMR 7588, France*
[3]*Synchrotron SOLEIL, L'Orme des Merisiers, Saint Aubin-BP 48, 91192 Gif sur Yvette Cedex, France*
[4]*Max-Plank-Institut für Festkrperforschung, D-70569, Stuttgart, Germany*

(Dated: January 25, 2012)

The structural and electronic properties of a Pb monolayer (ML) grown on Au(111) are investigated by ARPES and STM. Pb forms two domains rotated by $\pm 5^\circ$ with respect to the substrate. The resulting interface is an incommensurate moiré structure with an approximate unit cell of (6×6) R21.5°. Several Pb induced bands are observed with distinct orbital characters and different symmetries. The p_{xy} states cannot be described in a freestanding Pb ML picture: one of them clearly displays the two domains symmetry of the adlayer while the second follows the symmetry of the substrate. These are interpreted as arising from different degrees of hybridization of the Pb bands with the Au(111) substrate continuum.

I. INTRODUCTION

Angle resolved photoelectron spectroscopy (ARPES) with the advent of parallel high resolution angular detection is a powerful technique for the investigation of novel electronic properties in the band structure of solids [1]. Namely ARPES has been applied for the study of conflicting symmetries and multiple periodicities in the electronic band structure of solids [2]. In particular, systems displaying charge and spin density waves (CDW, SDW), with commensurate or incommensurate wave vectors, have been paradigm cases for the study of band topologies and conflicting periodicities [3–5]. Recently, complex surface super-periodicities have been observed not only at metal-metal interfaces [6], but also for boron-nitride and graphene grown on metallic substrates [7–14]. In these cases, ARPES has direct access to the results of the interplay between different symmetries and periodicities.

Pb overlayers have been studied in detail to unravel surfactant effects at the base of homo-epitaxial growth on Cu [15, 16]. Due to its high compressibility, a monolayer (ML) of Pb forms dense moiré superstructures. The corrugation of the adlayer and the expanded atomic distance with respect to the topmost substrate layer, yield a reduced vertical bonding strength with the latter [17]. The use of constant energy maps and quantitative analysis of the single-particle spectral function from ARPES data, has enabled the investigation of the electronic properties and the coherence length of a melting Pb layer on Cu(111) [18]. Recently unexpected superconductivity has been suggested in the 4/3 ML dense phase of Pb on Si(111) by means of scanning tunneling microscopy and spectroscopy (STM/STS) [19, 20].

In the present study of a Pb ML on Au(111), STM topography and LEED evidence an incommensurate moiré structure with an approximate (6×6) R21.5° unit cell, consisting of two Pb domains rotated by $\pm 5^\circ$ with respect to the Au(111) substrate. In the ARPES spectra three Pb induced bands are observed. The use of constant energy maps (CE maps) and a related tight-bidning model calculation reveal that two of the latter states have mainly p_{xy} character, one of which follows the periodicity and symmetry of the substrate, while the other does not. On the other hand, the third Pb derived state, with mainly p_z character, is strongly broadened in energy and momentum. Similar behavior has already been observed for other Pb MLs. In the case of Pb ML on Ag(111) [6] and Pb ML on Cu(111) [15]. These peculiar features of the three Pb induced bands are interpreted as arising from their orbital dependent hybridization with the substrate continuum.

II. EXPERIMENT

Au(111) has been cleaned by several cycles of sputtering (with Ar^+ at 300 K, 1keV for 30 minutes) and annealing (800 K for 25 minutes). In ARPES experiments, the cleanliness of the surface was verified by low energy electron diffraction (LEED) and ARPES measurements of the spin split surface states. Pb was evaporated (at 300 K with a flux of 0.33ML/min) from a calibrated EFM3 Omicron evaporator. The structural quality was improved by post-annealing at 400 K, and it was controlled by means of LEED. ARPES mesurements have been performed at room temperature (RT) with a Specs Phoibos 150 analyzer. The experimental energy resolution was set at 10 meV. The UV light source is a monochromatized high brightness GammaData VUV 5000 operating at the HeIα (21.22 eV) line. STM experiments have been performed in a separated UHV system equipped with home-built 0.4 K STM. The sample temperature in the experiment was 4 K, and the indicated bias voltage refers to the sample.

III. RESULTS

STM reveals large terraces of the adlayer with a characteristic periodic modulation. Figure 1**a** shows a constant-current STM image of the Pb monolayer on Au(111). The STM image presents an atomic resolution of the topmost layer

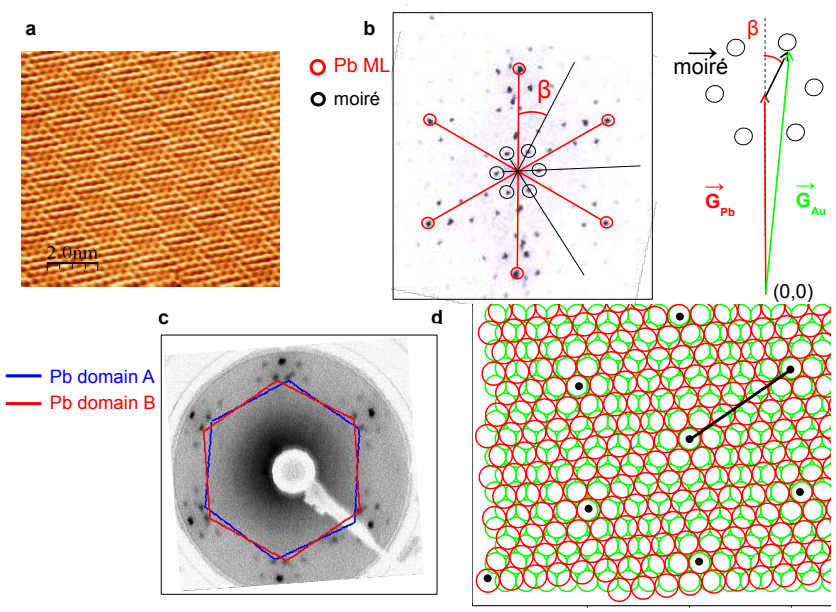

FIG. 1: (color online) **a** Constant current STM image of 1 ML Pb on Au(111), showing one rotational domain of the (6×6) R21.5° moiré structure (V_t = 2.0 V and I = 0.14 nA, T = 4.2 K). **b** Fourier transform of a larger scale (20×20 nm^2) STM data-set: the highest intensity spots enclosed in red circles are associated with the periodicity of the Pb adlayer. The moiré superstructure spots are indicated by black circles. The corresponding unit cell is rotated by β = 26.5° ± 1° and its fundamental vector is 4.74 times smaller than the (1,0) lattice vectors of Pb. The angle of rotation between the Pb ML and Au substrate is equal to 5° ± 0.2°. By using the Au substrate as a reference we can infer a structure close to (5.77×5.77) R21.5°. The inset of panel **b** is a cartoon of the reciprocal lattice vectors associated to the Au substrate, to one Pb domain and to the moiré superlattice. **c** LEED image of the moiré: blue and red lines trace the two hexagonal Pb domains. A rotation of ±5° is found between the Au substrate and the two rotational domains: the lengths and position of the reciprocal lattice vectors are in agreement with the STM results. **d** Structural model of the Pb monolayer (green circles represent the Au substrate, while red circles correspond to one of the two rotational Pb domains). In the model the moiré periodicity has been approximated to the closest commensurate structure.

and the long-range period created by the moiré pattern. This long periodicity is studied thoroughly in the reciprocal space. Figure 1**b** shows the Fourier transform map obtained from a larger scale STM image (20×20 nm^2) [21]. The analysis of the characteristic lengths and angle between the periodicities enables us to classify the PbAu(111) moiré as a (5.77×5.77) R21.5° with respect to the Au substrate lattice. In the rest of the article, for simplicity, the periodicity is referred to as a (6×6) R21.5°. The rotation between the moiré and the atomic lattices is compatible with a rotation of 5° between the Pb and the Au lattice [22]. The inset of **b** shows a cartoon of the characteristic lengths of the reciprocal lattice vectors and the angles between them. Figure 1**c** reports a LEED image of the Pb/Au(111) interface. The data suggests the existence of two possible Pb domains with a rotation of + and - 5° with respect to the substrate. The highest intensity spots are the first order diffraction spots of the Au substrate. Next to each of these, two weaker spots are visible. The latter are associated to the two distinct Pb domains and blue and red lines delineate the hexagonal unit cells of the two rotational Pb domains. Moreover, the presence of higher order diffraction spots ensure the good crystalline quality of the interfaces subject of the ARPES measurements. Figure 1**d** shows a geometrical model for the (6×6) interface: one single Pb adlayer (red circles) is overimposed to the Au substrate (green circles), with a rotation between the two lattices equal to 5°. The moiré is oversimplified and the periodicity is approximated to the closest commensurate periodicity, which requires a further 3% Pb lattice expansion and a further rotation of 4°.

We describe in the following the experimental band structure arising from the interaction of the Pb ML with the Au(111) substrate. The Fermi Surface (FS) of the interface is shown in Fig. 2**a**. This image is composed of data obtained by measurements along $\overline{\Gamma K}$ and two inequivalent $\overline{\Gamma M}$ high symmetry directions. A green hexagon defines the substrate Brillouin zone (BZ) while the smaller red and blue hexagons delimit the two Brillouin zones of Pb monolayer rotated of ±5°. The highest intensity is related to the bulk Au *sp* valence band state, while all the other features are Pb induced. Figure 2**b** displays a schematization of the Fermi Surface arising from bands with mainly Pb origin. The high symmetry points and the Pb states are indicated to guide the eye of the reader. Previous tight binding calculations performed for dense Pb monolayers on Cu(111) and Ag(111) [6, 15, 18], predict the presence of three Pb derived states with p_z orbital character, hereafter labelled Pb1, and with p_{xy} character, labelled Pb2 and Pb3. The same bands have been experimentally observed and they are depicted in the following. Close to the $\overline{\Gamma}$ point

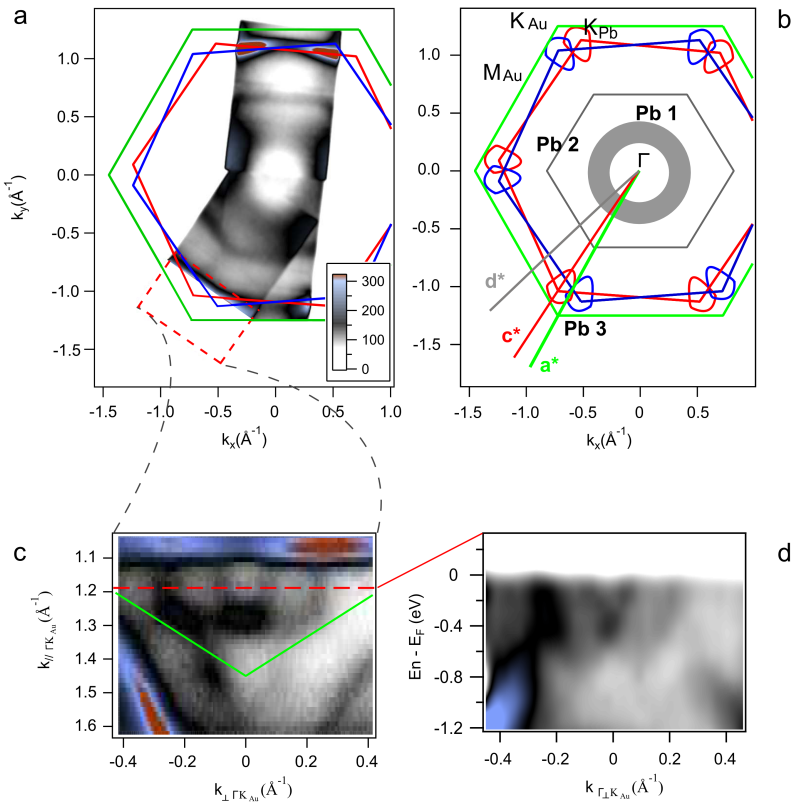

FIG. 2: (color online) **a** Fermi surface map obtained by combining CE maps along the $\overline{\Gamma M}_{Au}$ and $\overline{\Gamma K}_{Au}$ directions. The green hexagon follows the Au(111) surface BZ, while the two smaller blue and red hexagons define the two Pb BZs, with a rotation of $\pm 5^\circ$ with respect to the substrate. **b** Cartoon of the Pb derived Fermi surface: three lines with different colors, labelled **a***, **c*** and **d*** trace the directions of the cuts presented in panels **b**-**d** of Figure 3 (respectively $\overline{\Gamma K}_{Au}$, $\overline{\Gamma K}_{Pb}$ and 15° rotated with respect to $\overline{\Gamma K}_{Au}$). The first state (Pb1) appears in the Fermi surface map as a blurred circle close to the $\overline{\Gamma}$ point. The second one (Pb2) constitutes a well defined hexagon, displaying the substrate symmetry. In panel **a** a red dashed rectangle defines the region of the Fermi surface shown with higher detail in panel **c**. In panel **c** the outer Pb derived state (Pb3) is clearly visible; red and blue lines trace the position of the Pb3 derived pockets at the respective $\overline{K}$ points belonging to the BZs of the two rotational Pb domains. Panel **d** shows the band dispersion along a cut orthogonal to $\overline{\Gamma K}_{Au}$, traced in **c** with a red dashed line. The two-domain contribution on the Pb3 states is clearly depicted.

we observe a broad, almost circular, state, Pb1. At larger k values we see straight sections, associated to the Pb2 state, which forms a hexagon, as schematized in **b**. In panel **a** a dashed red rectangle encloses the region of the Fermi Surface which is shown in more detail in panel **c**. In the latter, close to the $\overline{K}_{Pb}$ of the two rotational domains of Pb, one may observe a circular pocket related to the Pb3 band (in panel **b** two distinct colors are used to distinguish the two Pb domains contributions). A red dashed line, orthogonal to $\overline{\Gamma K}_{Au}$, traces the direction of the cut in the band dispersion shown in panel **d**. In the latter, the two domains contribution of Pb3 is clearly depicted.

The behavior of the three Pb derived states is more clearly described by observing the energy dispersion of the bands reported in Figs. 2**a**-**c**-**d**. The three panels show cuts along $\overline{\Gamma K}_{Au}$, $\overline{\Gamma K}_{Pb}$ and 15° out of $\overline{\Gamma K}_{Au}$ respectively (with $\overline{\Gamma K}_{Au}$ = 1.45Å^{-1} and $\overline{\Gamma K}_{Pb}$ = 1.19Å^{-1}. The direction of the cuts is traced in Fig. 3**b** with three lines labelled **a***, **c*** and **d*** respectively. Figure 3**b** displays a sketch of the band structure along $\overline{\Gamma K}_{Au}$: the dispersion of the Au *sp* state and the projected bulk band gap as reported in [23] are also included. In Figures 3**a**-**c**-**d** the highest intensity state is the Au *sp* state, as observed in the FS. In Figures 3**a** and **c**, with the help of panel **b**, it is possible to identify the three Pb derived bands crossing the Fermi level. The first band, labelled Pb1 with k_{F1} = 0.35Å^{-1}, disperses with positive mass reaching its local minimum at the $\overline{\Gamma}$ point and displays strong broadening in energy and momentum, similar to what has been observed on PbAg(111) [6]. This broadening is responsible for the blurring of the resulting circular contour at the Fermi level in Figs. 2**a** and 2**b**.

At larger k values, the Pb2 state crosses the Fermi Level along $\overline{\Gamma K}_{Au}$ at k_F = 0.67Å^{-1}. The Pb2 band is sharper than Pb1 but the intensities of the two are comparable. The former crosses the Au *sp* state at -1.3eV and k = 0.89Å^{-1} and displays a significantly higher intensity after the crossing. Along $\overline{\Gamma K}_{Au}$ the dispersion of Pb2 shows a gap close to the BZ boundary of a freestanding Pb ML, near the minimum of the

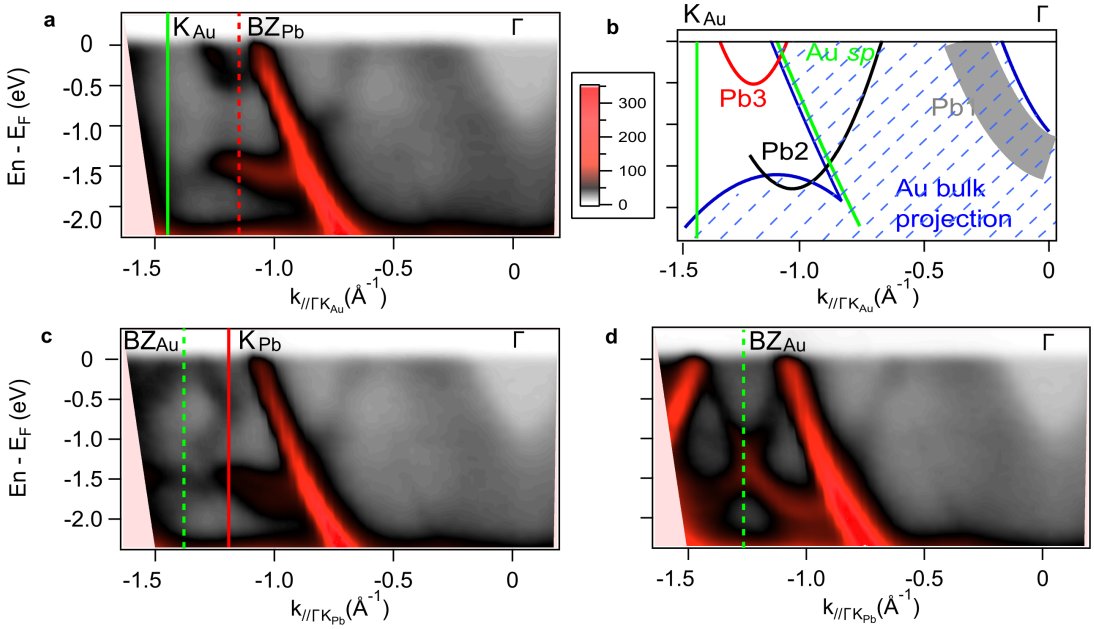

FIG. 3: (color online)**b** Sketch of the band structure along $\overline{\Gamma K}_{Au}$ where the position of the three Pb induced bands is reported. The dispersion of the Au *sp* state and the projected bulk band gap as reported in Ref. 23 are also reported. Panels **a**-**c**-**d** report respectively the band dispersion along $\overline{\Gamma K}_{Au}$, $\overline{\Gamma K}_{Au}$and 15° rotated with respect to $\overline{\Gamma K}_{Au}$. The positions of $\overline{K}_{Au}$ and $\overline{K}_{Pb}$ are traced with continuous green and red lines respectively. The borders of the Au and Pb BZs are indicated with dashed lines. In panel **b** and **c** a hybridization gap opens due to the interaction between the Pb2 and Pb3 states. The complete (un-gapped) dispersion of Pb2 and the its Umklapp replica are visible in **c**.

dispersion of the third Pb induced state, Pb3. Both the gap and the Pb3 band are absent in the band dispersion presented in Fig. 3**d** (15° off symmetry). This suggests that the gap observed in Fig. 3**a** results from the hybridization between Pb2 and Pb3. In Fig. 3**d** we observe the Umklapp replica of the Pb2 state, which is degenerate at the Fermi level with the Au *sp* state. The increase of the Pb2 intensity after the crossing of the Au *sp* state is even more pronounced in this figure.

The inner branch of the Pb2 state forms the hexagon in the CE map of Fig. 2**a**. Its outer branch is masked by the strong Au *sp* intensity. The third Pb induced band, labelled Pb3, has a parabolic dispersion with a positive effective mass. It gives rise to the small trigonally distorted circular pockets at the Brillouin zone $\overline{K}$ points of the two Pb rotational domains, more clearly visible in Fig. 2**c**. As a matter of fact, the Pb3 state follows the symmetry of the two rotational Pb domains. This is in striking contrast with the behavior of the Pb2 band, which displays the substrate symmetry. This symmetry difference, manifested by Pb states with nominally the same p_{xy} orbital character, represents a new finding, not reported in previous studies of a dense Pb ML [6, 15, 18].

In the present system we do not observe moiré-induced replica of the bands. This contrasts recent findings for graphene grown on metallic substrate [13, 14], for which the moiré gives rise to band replicas whose intensity reflects the strength of the superlattice potential. Therefore, in line with former observations [6, 15], we conclude that the moiré potential must have a comparatively smaller amplitude in the present case.

IV. DISCUSSION

The moiré periodicity and the interaction between the overlayer and the substrate are responsible for various peculiar features in the band structure of the PbAu(111) interface. The opening of a hybridization gap between Pb2 and Pb3 is clearly resolved in Figs. 3**a** and **c**. We have performed a model tight-binding calculation in order to elucidate the origin of this gap. Figure 4**a** shows the calculation results for p states arranged in a hexagonal lattice where the matrix elements are calculated using Slater-Koster energy integrals [24]. The resulting band structure mimics a freestanding Pb ML where one does not expect any hybridization between the p states due to their orthogonality. Similar oversimplified tight binding models have been used to analyze experimental results obtained for PbAg(111) and PbCu(111) [6, 15]. In agreement to these studies, there is no interaction gap between the p_{xy} states at the $\overline{K}$ point, nor between the p_{xy} and p_z states. A possible mechanism for the development of a hybridization is a partial intermixing of the symmetries of the Pb states. As already proposed in the case of PbCu(111) [15] this intermixing may originate from the buckling of the Pb layer. Figure 4**b** shows the tight binding calculation in the case of an asymmetric p_z state, following the methodology of Ref. 25. This z -asymmetry artificially mimics the presence of the underlying

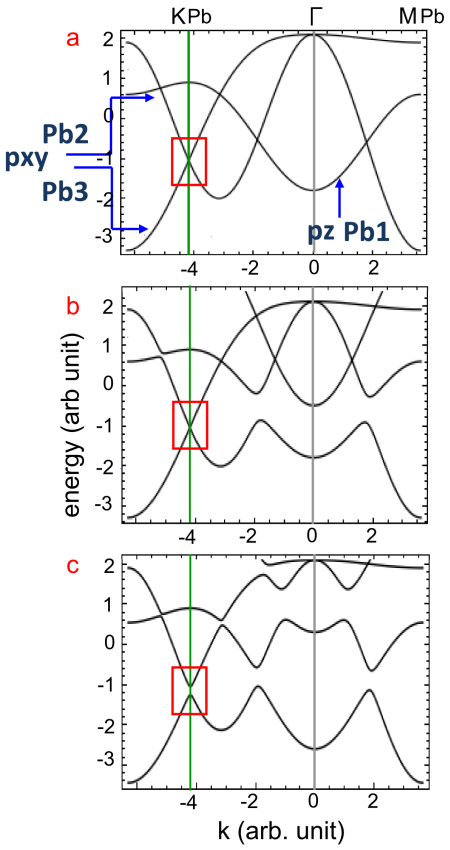

FIG. 4: (color online) **a** Calculated band structure for a tight binding model of p states arranged in a hexagonal 2D lattice as an equivalent to a freestanding Pb ML. Three bands are observed: two of them with p_{xy} orbital character and the third with p_z character, in agreement with previous tight binding calculation and our ARPES results [6, 15]. **b** The effect of an asymmetric p_z state, which mimics the presence of the underlying substrate. A gap opens between the p_{xy} and p_z states. **c** One possible way to lift the $\overline{\text{K}}$ degeneracy of the two p_{xy} states is to introduce the interaction between the Pb p states and the s state of the substrate, in the case of broken in-plane hexagonal symmetry (see text); a hybridization gap appears between the Pb2 and Pb3 states, similarly to our ARPES experimental results. The parameter values of the tight binding model are summarized in the Appendix.

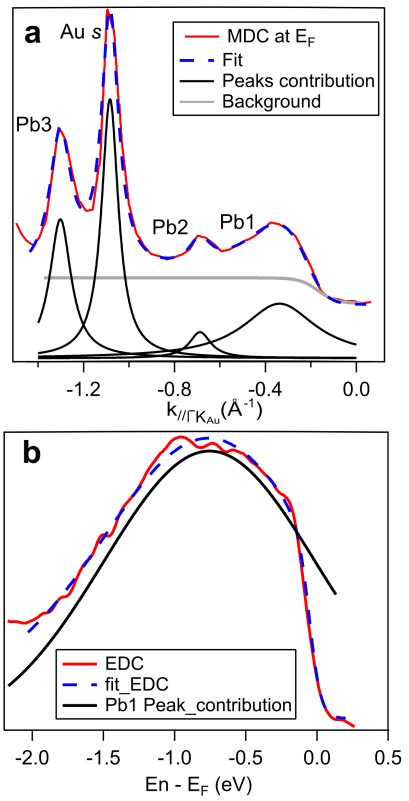

FIG. 5: (color online) **a** Momentum distribution curve (MDC) at the Fermi Level along $\overline{\Gamma\text{K}}_{\text{Au}}$. The fit is composed of four Lorentzians with widths: Pb1 0.39Å^{-1}, Pb2 0.11Å^{-1}, Pb3 0.11Å^{-1} and Au *sp* 0.08Å^{-1}. The four Lorentzian peaks are displyed under the MDC. The background contribution (light gray) shows the step-like shape used to reproduce the Au gap close to the $\overline{\Gamma}$ point. **b** Energy distribution curve (EDC) at k = -0.13Å^{-1} along $\overline{\Gamma\text{K}}_{\text{Au}}$ after the removal of a Shirley background. The Pb1 state is fitted with a Gaussian width of 1.748 $\pm$ 0.13 eV.

substrate, allowing the interaction of p_{xy} and p_z states and the opening of a hybridization gap between them. Nevertheless, the degeneracy of the two p_{xy} states at $\overline{\text{K}}$ is insensitive to any value of this z -asymmetry parameter.

One possible way to open a gap at the $\overline{\text{K}}$ point between the p_{xy} states (i.e. Pb2 and Pb3) is to extend the tight binding model in order to take into account an interaction between the p states and an s state of the substrate. Figure 4**c** shows the effect of this interaction in the case of broken in-plane hexagonal symmetry, i.e. nearest-neighbor substrate and overlayer interactions, where three substrate atoms are arranged on *hollow* sites determined by six overlayer atoms. In this case, a gap opens between the p_{xy} states at the $\overline{\text{K}}$ point, as observed experimentally in our ARPES results. Moreover, the interaction with the substrate breaks naturally the symmetry along the z axis, opening another hybridization gap between the p_{xy} and p_z states (i.e. no need of an artificial z -asymmetry parameter). The latter hybridization gap was previously reported for PbCu(111) [15], but it cannot be observed in the present ARPES results, due to the position of the band crossing above the Fermi level. The absence of degeneracy at $\overline{\text{K}}$ is a direct consequence of the broken in-plane symmetry, while a substantial value of *sp* hybridization is necessary for a non-negligible gap (see parameters in the Appendix). In the case of a cluster with hexagonal in-plane symmetry, there is no p_{xy} gap at $\overline{\text{K}}$ for any value of *sp* hybridization, as we have verified for (a) an atomic arrangement where overlayer atoms sit on *on-top* sites and (b) for *on-site sp* hybridization (data not shown).

We stress the fact that our model tight binding calculation represents an oversimplified picture of the real structure, aiming to a qualitative explanation of the main band structure features. Despite its simplicity it may well identify the inter-

action between the Pb *p* states and the substrate *s* state, and the necessity to break the nearest-neighbor in-plane hexagonal symmetry, as the two important ingredients. The in-plane hexagonal symmetry is indeed absent in the real PbAu(111) due to the incommensurate character of the interface.

The second characteristic in the band structure is the difference between the energy and momentum linewidth of Pb1 and the those of the other states. Figure 5 quantifies this momentum and energy broadening. Figure 5**a** shows a momentum distribution curve (MDC) at E_F, along $\overline{\Gamma K}_{Au}$ displaying the three Pb peaks and the Au *sp* band. The curve can be fitted by four Lorentzians, albeit with a three times larger width for Pb1 in comparison the other peaks (see Fig. 5 for the corresponding values). The EDC at k = -0.13Å^{-1} displays the Pb1 peak after background removal. This strong background is probably due to the contribution of an indirect transition; its photointensity is proportional to the one-dimensional density of states of the initial state integrated along k_z [26]. The Pb1 peak is fitted with a Gaussian having a width of 1.74 $\pm$ 0.13 eV. This value is large and comparable to the one of 1.86 eV reported for a Pb ML on Ag(111) [6].

The effect of the aforementioned moiré periodicity, and the resulting inequivalence of Pb absorption sites in the nearly commensurate superstructure, is equivalent to disorder. But such an effect is not strong enough to explain the energy and momentum broadening of Pb1. As pointed out for a Pb ML on Ag(111) [6], it is necessary to consider a second mechanism: the hybridization of the p_z state with the Au surface state. When hybridized, the Pb band, acquires a longer penetration depth in the substrate and presents a stronger interaction with the bulk continuum. The latter which contributes to the spectral weight spreading around the Pb1 band dispersion: this is analogous to an impurity interacting with a continuum.

A third unexpected, and precedently unreported, feature in the band structure of the Pb ML on Au(111) is the symmetry difference of the the CE contours between the two p_{xy} derived bands. This peculiarity becomes clear by the CE maps of Fig. 2. The Pb3 state becomes apparent as two pockets centered around the respective $\overline{\text{K}}$ points of the BZs of the two rotational Pb domains; in Fig. 2**b** they are traced by red and blue lines. By contrast, the Fermi contour constituted by Pb2, as can be seen in Fig. 2**a**, is a single hexagon. Therefore the symmetry of Pb2 is that of the substrate and not the one of the overlayer. On the other hand, the symmetry of the Fermi contour attributed to Pb1 state is undetermined because of the blurring induced by the band broadening.

We interpret the different band symmetry of the p_{xy} derived states as arising from a different degree of hybridization of the Pb2 and Pb3 bands with the Au continuum. We have previously shown that such an interaction between the p_{xy} states and substrate *s* state is a key ingredient for explaining the opening of the hybridization gap between Pb2 and Pb3 at the $\overline{\text{K}}$ point. Our tight binding model has also evidenced that Pb2 interacts and hybridizes with Pb1. Hence, the former can acquire a partial p_z character. The p_z orbital component can strongly interact with the substrate continuum through hybridization with the surface state [6]. For this reason we propose that the strength of the interaction between the substrate *s* state and the Pb p_{xy} states is stronger in the case of Pb2 and weaker for Pb3.

The last point to be addressed is the different band intensity for k values smaller or larger than the Au *sp* crissing. Before crossing with the Au band, the spectral weight of the Pb1 and Pb2 states, is small compared to the intensity of the Pb3 band and the branch of Pb2 outside the Au *sp* state (see Fig. 3**a**-**c**-**d**). This is another consequence of a different degree of interaction between the Pb derived bands and the substrate continuum. For larger k values, in fact, the bands enter in the projected bulk gap of the substrate, as it is displayed in Fig. 2**b** [23], hence the absence of bulk continuum makes it impossible for the Pb3 states to hybridize and delocalize according to the mechanism discussed above. The interaction strength, as well as and the penetration depth of the Pb2 wavefunction in the Au bulk continuum, are smaller than for Pb1. Pb1 is so strongly interacting with all the bulk continuum that the resulting energy spread blurs the constant energy contour. On the other hand, for Pb2 the longer penetration in the Au bulk continuum manifest itself as a change in the band structure. The Pb2 state feels much stronger the substrate symmetry, while Pb3 is more localized in the Pb overlayer and displays its two-domain symmetry.

V. CONCLUSIONS

We performed STM and ARPES measurements on the Pb ML on Au(111). Our observations show a peculiar orbital selective interaction of three Pb derived bands with the bulk continuum of the substrate.

Interestingly, the two p_{xy} derived bands have distinctively different symmetries; while the first (Pb2) follows the substrate symmetry, the second (Pb3) is linked to the symmetry of the overlayer. As captured by a model tight binding calculation, the Pb2 state has not only a p_{xy} character, but there is also a small amount of p_z character due to the interaction with Pb1. The p_z component can hybridize with the s band and the Au surface state, thus increasing the penetration depth of the state in the bulk continuum. The intermixing of the Pb p orbital with the substrate s state may also explain the hybridization gap between the Pb2 and Pb3 band, as reproduced by our tight-binding calculation in the case of sp interaction. For the Pb1 band the selective hybridization broadens the state in such a strong way that the blurred Fermi level contour does not allow for a unique identification of the underlying symmetry. While the broadening effect is weaker for Pb2, one can still observe the effect of delocalization in the bulk as a change in the band structure itself which follows the substrate symmetry. A similar interaction mechanism is impossible for Pb3 because it lies entirely within the projected band gap of the Au substrate.

APPENDIX

The different hybridization strengths used in the tight binding model presented in Fig. 4 are summarized in the following Table.

TABLE I: Hybridization parameters following the notation of Ref. 24 and corresponding absolute energy values in units of ($pp\sigma$).

Parameters	Fig. 4**a**	Fig. 4**b**	Fig. 4**c**
($pp\sigma$)	1	1	1
($pp\pi$)	0.3	0.3	0.3
($ss\sigma$)	N/A	N/A	0.5
($sp\sigma$)	N/A	N/A	0.5
z-asymmetry	0	0.1	0

* Electronic address: alberto.crepaldi@epfl.ch

[1] A. Damascelli, Z. Hussain, and Z.-H. Shen, Rev. Mod. Phys. **75**, 473 (2003).

[2] M. Grioni, C. R. Ast, D. Pacilé, M. Papagno, H. Berger, and L. Perfetti, New J. Phys **7**, 106 (2005).

[3] J. Voit, L. Perfetti, F. Zwick, H. Berger, G. Margaritondo, G. Grüner, H. Hochst, and M. Grioni, Science **290**, 501 (2000).

[4] J. Schäfer, E. Rotenberg, G. Meigs, S. D. Kevan, P. Blaha, and S. Hüfner, Phys. Rev. Lett. **83**, 102069 (1999).

[5] L. X. Yang, Y. Zhang, H. Ou, J. F. Zhao, D. Shen, B. Zhou, J. Wei, F. Chen, M. Xu, C. He, et al., Phys. Rev. Lett. **102**, 107002 (2009).

[6] C. R. Ast, D. Pacilé, M. Papagno, T. Gloor, F. Mila, S. Fedrigo, G. Wittich, K. Kern, H. Brune, and M. Grioni, Phys. Rev. B **73**, 245428 (2006).

[7] T. Brugger, S. Günther, B. Wang, J. H. Dil, M.-L. Bocquet, J. Osterwalder, J. Wintterlin, and T. Greber, Phys. Rev. B **79**, 045407 (2009).

[8] M. Corso, W. Auwärter, M. Muntwiler, A. Tamai, T. Greber, and J. Osterwalder, Science **303**, 217 (2004).

[9] R. Laskowski, P. Blaha, T. Gallauner, and K.Schwarz, Phys. Rev. Lett. **98**, 106802 (2007).

[10] A. T. N'Diaye, S. Bleikamp, P. J. Feibelman, and T. Michely, Phys. Rev. Lett. **97**, 215501 (2006).

[11] S. Marchini, S. Günther, and J. Wintterlin, Phys. Rev. B **76**, 075429 (2007).

[12] T. Land, T. Michely, R. Behm, J. Hemminger, and G. Comsa, Surf. Sci. **264**, 261 (1992).

[13] I. Pletikosic, M. Kralj, P. Pervan, R. Brako, J. Coraux, A. T. N'Diaye, C. Busse, and T. Michely, Phys. Rev. Lett. **102**, 056808 (2009).

[14] S. Rusponi, M. Papagno, P. Moras, S. Vlaic, M. Etzkorn, P. M. Sheverdyaeva, D. Pacilé, H. Brune, and C. Carbone, Phys. Rev. Lett. **105**, 246803 (2010).

[15] F. Baumberger, A. Tamai, M. Muntwiler, T. Greber, and J. Osterwalder, Surf. Sci. **532-535**, 82 (2003).

[16] J. Camarero, J. Ferrón, V. Cros, L. Gómez, A. L. V. de Parga, J. M. Gallego, J. E. Prieto, J. J. de Miguel, and R. Miranda, Phys. Rev. Lett. **81**, 850 (1998).

[17] N. Tsud, S. Fabik, V. Dudr, M. Vondracek, V. Chab, V. Matolin, and K. Prince, Surf. Sci. **542**, 112 (2003).

[18] F. Baumberger, W. Auwärter, T. Greber, and J. Osterwalder, Science **306**, 2221 (2004).

[19] S. Qin, J. Kim, Q. Niu, and C.-K. Shih, Science **324**, 1314 (2009).

[20] T. Zhang, P. Cheng, W.-J. Li, Y.-J. Sun, G. Wang, X.-G. Zhu, K. He, L. Wang, X. Ma, X. Chen, et al., Nat. Phys. **6**, 104 (2010).

[21] I. Horcas, R. Fernndez, J. M. Gmez-Rodrguez, J. Colchero, J. Gmez-Herrero, and A. M. Baro, Rev. Sci. Instrum. **78**, 013705 (2007).

[22] T. Wiederholt, H. Brune, J. Wintterlin, R. Behm, and G. Ertl, Surf. Sci. **324**, 91 (1995).

[23] R. Mazzarello, A. D. Corso, and E. Tosatti, Surf. Sci. **602**, 893905 (2008).

[24] J. C. Slater and G. F. Koster, Phys. Rev. **94**, 1498 (1954).

[25] L. Petersen and P. Hedegard, Surf. Sci. **459**, 49 (2000).

[26] M. Lindroos and A. Bansil, Phys. Rev. Lett. **77**, 14 (1996).